EMAP5: A 3D HYBRID FEM/MOM CODE

Y. Ji and T. Hubing
Department of Electrical and Computer Engineering
University of Missouri-Rolla
Rolla, MO 65401

Abstract--EMAP5 is a numerical software package designed to model electromagnetic problems. It employs the finite element method (FEM) to analyze a volume, and employs the method of moments (MoM) to analyze the region exterior to the FEM volume. The two methods are coupled by enforcing the continuity of the tangential fields on the interface. Dielectrics, lossy dielectrics and metal objects can be modeled within the FEM volume. Metal objects can also be located exterior to, or on the surface of the FEM volume. A simple input file translator (SIFT) is provided with EMAP5 that allows users to define basic input configurations on a rectangular grid without a graphical interface. It is also possible to use commercial mesh generators to analyze more complex geometries of arbitrary shape. EMAP5 can model three types of sources: incident plane waves, voltage sources on metal patches and impressed current sources in the finite element region. This paper describes the implementation of EMAP5 and provides four examples to demonstrate the range of configurations that EMAP5 is capable of modeling using the SIFT translator.

I.   INTRODUCTION

Methods used to solve Maxwell's equations can often be classified into one of two categories. One category is integral equation-based methods. Integral equation-based methods generally solve for unknown fields or currents on the surface of homogeneous volumes. Only the surfaces are meshed; therefore the number of unknowns is relatively small. Integral equation-based methods are well suited for modeling homogeneous structures in unbounded geometries.

The other category is partial differential equation (PDE) -based methods. PDE-based methods require a volume mesh. The resulting number of unknowns is usually much higher than that obtained from integral equation-based methods, but the reduced complexity of the solution method can more than compensate for this. PDE-based methods are well suited for modeling complex inhomogeneous structures, particularly those in bounded geometries (e.g. a waveguide or a metallic enclosure).

The finite element method (FEM) is a powerful PDE-based method. It requires the entire region of interest to be meshed. However, each mesh element can have its own electromagnetic properties (ε, μ, σ).

Thus, FEM has an inherent capacity to analyze inhomogeneous structures. In addition, FEM does not require a uniform mesh. Various types of elements, for example, bricks, tetrahedra and prisms, can be used to discretize arbitrary geometric configurations. Therefore, FEM is well suited for modeling complex, inhomogeneous structures. A significant disadvantage of the FEM method is the inability to model unbounded geometries without using absorbing boundary elements. Absorbing boundary elements are not effective when they closely conform to the shape of long thin objects (e.g. cables). When modeling objects with one dimension significantly longer than the others using FEM, it is generally necessary to fill the empty space around these objects with many elements that transition from the object of interest to the absorbing boundary. This can significantly inflate the overall size of the problem.

The method of moments is not actually an electromagnetic modeling technique, but rather it is a technique for solving complex linear equations [1, 2]. However, electromagnetic modeling techniques that apply the method of moments to the solution of electric or magnetic field integral equations are generally referred to as method-of-moment (MoM) techniques. MoM techniques can be used to model metallic (particularly wire) structures in unbounded geometries very effectively.

In order to take advantage of the strengths of both the FEM and MoM methods, several researchers have developed hybrid FEM/MoM approaches [3-6]. Hybrid FEM/MoM methods generally take advantage of the FEM's ability to model complex inhomogeneous structures and the MoM's ability to model unbounded geometries. The specific strengths of a particular code depend on the details of the implementation, particularly the form of the integral equation and the basis and weighting functions employed.

EMAP5 (**E**lectro **M**agnetic **A**nalysis **P**rogram version **5**) is a hybrid FEM/MoM modeling code developed at the University of Missouri-Rolla (UMR). EMAP5 was developed in order to demonstrate and validate the hybrid technique described in [6,7]. This technique, used in conjunction with a mesh generator, is particularly useful for analyzing EMI from printed circuit board geometries with enclosures or attached cables. A rudimentary mesh generator (SIFT5) is distributed with the EMAP5 code. This non-graphical

user interface is simple and portable, making it a good tool for educators and people who want to learn to use the EMAP5 code. However, the meshes generated by the SIFT5 code do not exploit the primary advantage of FEM modeling codes (i.e. the ability to adapt the size and shape of the mesh to fit the geometry). The EMAP5 and SIFT5 source codes can be obtained via the web at <http://www.emclab.umr.edu/emap5>.

II.   FORMULATION

Although details of the EMAP5 formulation are described in [6,7], a brief summary is provided below. The general structure of interest is shown in Figure 1. A dielectric volume V_2 has electrical properties (ε_2, μ_2) and is enclosed by a surface S_2. A conductive volume V_3 is enclosed by a conductive surface S_c. The fields within V_3 vanish. V_1 denotes the volume outside of V_2 and V_3, which is assumed to be free space. (E_1, H_1) and (E_2, H_2) denote the electric and magnetic fields in V_1 and V_2, respectively. The unit normal vectors for S_2 and S_c are defined pointing outward toward V_1. The structure is excited by an incident wave (E^{inc}, H^{inc}) or impressed sources (J^{int}, M^{int}). The scattered electric and magnetic fields are (E^s, H^s). The objective is to solve for the scattered fields (E^s, H^s) or the surface electric current density on S_c.
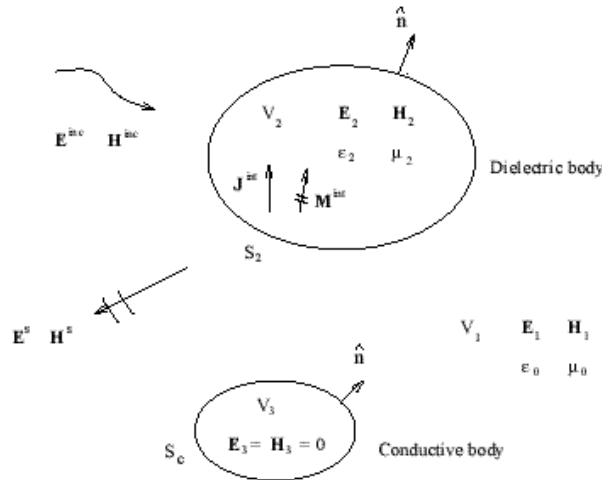

Figure 1. A dielectric object and a conductive object illuminated by (E^{inc}, H^{inc}) or (J^{int}, M^{int}).

From Maxwell equations, the vector Helmholtz equation in terms of E can be written as,

$$\nabla \times \left(\frac{\nabla \times E(r)}{j\omega\mu_0\mu_r} \right) + j\omega\varepsilon_0\varepsilon_r E(r)$$
$$= -J^{int}(r) - \frac{1}{j\omega\mu_0\mu_r}\nabla \times M^{int}(r). \tag{1}$$

After multiplying Equation (1) by a weighting function $w(r)$ and integrating over the finite element domain V_2, one obtains the FEM weak form as follows [8, 9],

$$\int_{V_2}\left[\frac{(\nabla \times E(r)) \bullet (\nabla \times w(r))}{j\omega\mu_0\mu_r} + j\omega\varepsilon_0\varepsilon_r E(r) \bullet w(r) \right] dV$$

$$= \int_{S_2} (\hat{n} \times H(r)) \bullet w(r)\, dS$$

$$- \int_{V_2}\left[J^{int}(r) + \frac{1}{j\omega\varepsilon_0\varepsilon_r}\nabla \times M^{int}(r) \right] \bullet w(r)\, dV \tag{2}$$

Equation (2) can also be derived using the variational method [10] (pp. 158-161), [11] (pp. 158-160).

Within volume V_2, EMAP5 uses the vector tetrahedral elements proposed by Barton and Cendes [10] (pp. 56-59), [12]. Each basis function is defined within a tetrahedron, and is associated with one of the six edges. The electric field E within volume V_2 can be expanded as,

$$E(r) = \sum_{n=1}^{N_V} E_n\, w_n(r) \tag{3}$$

where N_V is the total number of interior edges and boundary edges on the dielectric surface, and $\{E_n\}$ is a set of unknown complex scalar coefficients.

The surface integral term in Equation (2) can be evaluated by using a surface basis function $f(r)$, which is discussed later. The weighting functions chosen are $w_n(r)$, n=1…Nv. After multiplying by the weighting functions, Equation (2) can be discretized as,

$$\begin{bmatrix} A_{ii} & A_{id} \\ A_{di} & A_{dd} \end{bmatrix}\begin{bmatrix} E_i \\ E_d \end{bmatrix} = \begin{bmatrix} 0 & 0 \\ 0 & B_{dh} \end{bmatrix}\begin{bmatrix} 0 \\ J_h \end{bmatrix} + \begin{bmatrix} g^{int} \end{bmatrix} \tag{4}$$

The unknown coefficients $[E_n]$ are partitioned according to edge type. The two categories are interior edges, which are denoted by the subscript i in Equation (4), and dielectric boundary edges, which are denoted by the subscript d in Equation (4). $[J_h]$ is a set of unknown complex scalar coefficients for the surface electric current densities on S_d. S_d is defined as S_2 if the conductive body is not adjacent to the dielectric body; otherwise, $S_d = S_2 - (S_2 \cap S_c)$. Edges in $[J_h]$ include dielectric boundary edges and junction edges (i.e. edges that are on both the conductor and dielectric boundary). $[B_{dh}]$ is a square matrix if there are no junction edges in the problem. $[g^{int}]$ is the source term, representing sources located within the FEM region. The elements of $[A]$, $[B_{dh}]$, and $[g^{int}]$ are given by,

$$A_{mn} = \int_{V_2} \left[\frac{(\nabla \times \mathbf{w}_n(\mathbf{r})) \bullet (\nabla \times \mathbf{w}_m(\mathbf{r}))}{j \omega \mu_o \mu_r} + j \omega \varepsilon_o \varepsilon_r \mathbf{w}_n(\mathbf{r}) \bullet \mathbf{w}_m(\mathbf{r}) \right] dV \quad (5)$$

$$B_{mn} = \int_{S_d} \mathbf{f}_n(\mathbf{r}) \bullet \mathbf{w}_m(\mathbf{r}) \, dS \quad (6)$$

$$g_m^{int} = -\int_{V_2} \left[\mathbf{J}^{int} + \frac{1}{j \omega \mu_o \mu_r} (\nabla \times \mathbf{M}^{int}) \right] \bullet \mathbf{w}_m(\mathbf{r}) \, dV \quad (7)$$

where $\mathbf{f}_n(\mathbf{r})$ is the surface basis function. Since the tangential $\mathbf{E}$ field vanishes on S_c, B_{mn} is evaluated over S_d rather than all of S_2. A detailed description of how to evaluate the terms in Equation (5) is provided in [11] (pp. 254-257). Appendix A describes how to evaluate Equation (6). $[g^{int}]$ is the source term and is discussed in a later section.

The MoM surface integral equation evaluated by the MoM part of EMAP5 is a form of the electric field integral equation (EFIE) [13],

$$\mathbf{E}^{inc}(\mathbf{r}) = \frac{1}{2}\mathbf{E}(\mathbf{r}) + \oint_S \{ \mathbf{M}(\mathbf{r}') \times \nabla' G_0(\mathbf{r}, \mathbf{r}') \\ + j k_0 \eta_0 \mathbf{J}(\mathbf{r}') G_0(\mathbf{r}, \mathbf{r}') \\ - j \frac{\eta_0}{k_0} \nabla' \bullet \mathbf{J}(\mathbf{r}') \nabla' G_0(\mathbf{r}, \mathbf{r}') \} dS' \quad (8)$$

where $\mathbf{r} \in S$, $S \equiv S_c \cup S_2$, η_0 and k_0 are the intrinsic impedance and wavenumber in free space, respectively, and

$$G_0(\mathbf{r}, \mathbf{r}') = \frac{e^{-jk_0|\mathbf{r}-\mathbf{r}'|}}{4\pi|\mathbf{r}-\mathbf{r}'|} \quad (9)$$

is the Green's function in free space. The integral term with a bar in Equation (8) denotes a principal-value integral. The singularity at $\mathbf{r} = \mathbf{r}'$ is excluded. The equivalent surface electric and magnetic currents are defined as,

$$\mathbf{J}(\mathbf{r}) = \hat{\mathbf{n}} \times \mathbf{H}(\mathbf{r}), \qquad \mathbf{r} \in S \quad (10)$$

$$\mathbf{M}(\mathbf{r}) = \mathbf{E}(\mathbf{r}) \times \hat{\mathbf{n}}, \qquad \mathbf{r} \in S_d. \quad (11)$$

$\mathbf{M}(\mathbf{r})$ vanishes on S_c. $\mathbf{J}(\mathbf{r})$ and $\mathbf{M}(\mathbf{r})$ can be approximated by using the triangular basis function $\mathbf{f}_n(\mathbf{r})$ proposed by Glisson [14]. On the surface S_d, the MoM basis function $\mathbf{f}_n(\mathbf{r})$ and the FEM basis function $\mathbf{w}_n(\mathbf{r})$ are related by,

$$\mathbf{w}_n(\mathbf{r}) = \hat{\mathbf{n}} \times \mathbf{f}_n(\mathbf{r}), \qquad \mathbf{r} \in S_d \quad (12)$$

$\mathbf{J}(\mathbf{r})$, $\mathbf{M}(\mathbf{r})$ can be expanded as,

$$\mathbf{J}(\mathbf{r}) = \sum_{n=1}^{N_s} J_n \mathbf{f}_n(\mathbf{r}) \quad (13)$$

$$\mathbf{M}(\mathbf{r}) = \sum_{n=1}^{N_d} E_n \mathbf{f}_n(\mathbf{r}) \quad (14)$$

where N_s is the total number of edges on the surface S, and N_d is the total number of edges on the surface S_d. $\{J_n\}$ and $\{E_n\}$ are unknown complex scalar coefficients.

The weighting functions chosen are $\mathbf{f}_n(\mathbf{r})$, n=1, ... N_s. After multiplying by the weighting functions, Equation (8) can be discretized into Equation (15), which is a matrix equation. Edges on S_d and S_c are grouped together respectively.

$$\begin{bmatrix} C_{hh} & C_{hc} \\ C_{ch} & C_{cc} \end{bmatrix} \begin{bmatrix} J_h \\ J_c \end{bmatrix} = \begin{bmatrix} D_{hd} & 0 \\ D_{cd} & 0 \end{bmatrix} \begin{bmatrix} E_d \\ 0 \end{bmatrix} - \begin{bmatrix} F_h^i \\ F_c^i \end{bmatrix}. \quad (15)$$

The elements in matrices $[C]$, $[D]$ and $[F^i]$ are given by,

$$C_{mn} = -jk_0\eta_0 \int_{S_m} \mathbf{f}_m(\mathbf{r}) \bullet \left[\int_{S_n} \mathbf{f}_n(\mathbf{r}') G_0(\mathbf{r}, \mathbf{r}') dS' \right] dS \\ + j\frac{\eta_0}{k_0} \int_{S_m} \mathbf{f}_m(\mathbf{r}) \bullet \left[\oint_{S_n} (\nabla' \bullet \mathbf{f}_n(\mathbf{r}')) \nabla' G_0(\mathbf{r}, \mathbf{r}') dS' \right] dS \quad (16)$$

$$D_{mn} = \int_{S_m} \mathbf{f}_m(\mathbf{r}) \bullet \\ \left[\oint_{S_n} \mathbf{f}_n(\mathbf{r}') \times \nabla' G_0(\mathbf{r}, \mathbf{r}') dS' + \frac{1}{2} \mathbf{w}_n(\mathbf{r}) \right] dS \quad (17)$$

$$F_m^i = \int_{S_m} \mathbf{f}_m(\mathbf{r}) \bullet \mathbf{E}^{inc}(\mathbf{r}) \, dS. \quad (18)$$

Details of how to evaluate Equation (16) are provided in [14]. Appendix B describes how to evaluate Equation (17). Equation (18) can be evaluated by using the Gaussian Quadrature technique.

From Equation (15), $[J_h]$ can be expressed as,

$$\begin{bmatrix} 0 \\ J_h \end{bmatrix} = \begin{bmatrix} 0 & 0 \\ 0 & C'^{-1}_{hh} D'_{hd} \end{bmatrix} \begin{bmatrix} 0 \\ E_d \end{bmatrix} + \begin{bmatrix} 0 \\ C'^{-1}_{hh} K \end{bmatrix} \quad (19)$$

where

$$C'_{hh} \equiv C_{hh} - C_{hc} C_{cc}^{-1} C_{ch} \quad (20)$$

$$D'_{hd} \equiv D_{hd} - C_{hc} C_{cc}^{-1} D_{cd} \quad (21)$$

$$K \equiv C_{hc} C_{cc}^{-1} F_c^i - F_h^i. \quad (22)$$

After combining Equations (4) and (19), the final matrix equation that must be solved is given by,

$$\left([A] + \begin{bmatrix} 0 & 0 \\ 0 & -B_{dh}C_{hh}'^{-1}D_{hd}' \end{bmatrix} \right) \begin{bmatrix} E_i \\ E_d \end{bmatrix} \tag{23}$$
$$= [g^{\text{int}}] + \begin{bmatrix} 0 \\ B_{dh}C_{hh}'^{-1}K \end{bmatrix}$$

where $[A]$ is the FEM matrix in Equation (4), and $B_{dh}C_{hh}^{-1}D_{hd}'$ is the coupled matrix from the MoM equation. The right-hand side in Equation (23) is the source term.

The far fields can be calculated using the equivalent surface currents **J** and **M** defined in Equations (10) and (11). The point of observation is denoted by (r, θ, φ) in spherical coordinates. Potential functions **A** and **F** can be approximated by [15],

$$\mathbf{A}(\mathbf{r}) \cong \frac{e^{-jk_0\mathrm{r}}}{4\boldsymbol{p}\mathrm{r}} \int_S \mathbf{J}(\mathbf{r}') e^{jk_0 \mathrm{r}'\cos\boldsymbol{y}} dS'$$
$$= \frac{e^{-jk_0\mathrm{r}}}{4\boldsymbol{p}\mathrm{r}} \sum J_n \int_{S_n} \mathbf{f}_n(\mathbf{r}') e^{jk_0 \mathrm{r}'\cos\boldsymbol{y}} dS' \tag{24}$$

$$\mathbf{F}(\mathbf{r}) \cong \frac{e^{-jk_0\mathrm{r}}}{4\boldsymbol{p}\mathrm{r}} \int_S \mathbf{M}(\mathbf{r}') e^{jk_0 \mathrm{r}'\cos\boldsymbol{y}} dS'$$
$$= \frac{e^{-jk_0\mathrm{r}}}{4\boldsymbol{p}\mathrm{r}} \sum E_n \int_{S_n} \mathbf{f}_n(\mathbf{r}') e^{jk_0 \mathrm{r}'\cos\boldsymbol{y}} dS' \tag{25}$$

where $\mathrm{r}'\cos\boldsymbol{y} = \mathrm{x}'\cos\boldsymbol{j}\,\sin\boldsymbol{q} + \mathrm{y}'\sin\boldsymbol{j}\,\sin\boldsymbol{q} + \mathrm{z}'\cos\boldsymbol{q}$. EMAP5 evaluates the integral terms in Equations (24) and (25) using the Gaussian Quadrature technique. The far fields are given by [15],

$$E_{\boldsymbol{q}} = (-j k_0 \boldsymbol{h}_0)(A_{\boldsymbol{q}} + \frac{F_{\boldsymbol{j}}}{\boldsymbol{h}_0}) \tag{26}$$

$$E_{\boldsymbol{j}} = (-j k_0 \boldsymbol{h}_0)(A_{\boldsymbol{j}} - \frac{F_{\boldsymbol{q}}}{\boldsymbol{h}_0}). \tag{27}$$

III. SOURCE AND LOAD MODELING

EMAP5 can model voltage sources on metal patches, incident plane waves, and impressed current sources within the FEM region. A delta-gap voltage source can be defined anywhere on the MoM surface. It can be modeled as an incident E-field normal to edges coinciding with the source [9] (pp. 260-261). A delta-gap voltage source parallel to the x-axis can be expressed as,

$$\mathbf{E}^{\text{inc}} = V\boldsymbol{d}(x - x_f)\vec{x} \tag{28}$$

where x_f is the location of the source and V is the voltage magnitude, and $\boldsymbol{d}(x)$ is the Dirac delta function. Suppose that edge m coincides with the source. The normal component of $\mathbf{f}_m(\mathbf{r})$ across edge m is unity. Thus, the source term given by Equation (18) is,

$$F_m^i = V l_m \tag{29}$$

where l_m is the length of edge m.

Plane wave sources are also described using the forcing term given by Equation (18). Assume the incident wave can be expressed in a spherical coordinate system as,

$$\mathbf{E}^{\text{inc}} = (E_{\boldsymbol{q}}\hat{\boldsymbol{q}} + E_{\boldsymbol{j}}\boldsymbol{j}) e^{-j\mathbf{k}\cdot\mathbf{r}} \tag{30}$$

where the propagation vector **k** is,

$$\mathbf{k} = k(\sin\boldsymbol{q}\cos\boldsymbol{j}\,\hat{\mathbf{x}} + \sin\boldsymbol{q}\sin\boldsymbol{j}\,\hat{\mathbf{y}} + \cos\boldsymbol{q}\hat{\mathbf{z}}) \tag{31}$$

and $(\boldsymbol{q},\boldsymbol{j})$ defines the angle of the propagation direction of the plane wave. EMAP5 calculates the E field of the plane wave on the surface of the structure, then evaluates the right-hand side of Equation (18) numerically.

EMAP5 uses current filaments on tetrahedron edges to model sources located within the FEM region [11] (pp. 324-325). A current source along the z-axis can be expressed as,

$$\mathbf{J}^{\text{int}} = I \boldsymbol{d}(x - x_f)\boldsymbol{d}(y - y_f)\hat{\mathbf{z}} \tag{32}$$

where (x_f, y_f) specifies its position, I denotes the electric current magnitude, and $\boldsymbol{d}(x)$ is the Dirac delta function. The contribution to vector $[g^{\text{int}}]$ in Equation (7) is simply,

$$g^{\text{int}} = I l \iint \hat{\mathbf{z}}\bullet\{W\}\boldsymbol{d}(x - x_f)\boldsymbol{d}(y - y_f)\,dx\,dy \tag{33}$$

where l is the edge length and $\{W\}$ is the weighting function. According to the expression in Equation (33), only edges coinciding with a current source have non-zero components in the $[g^{\text{int}}]$ vector. After the E-fields along the current source edges are obtained, the voltage drop across the source can be calculated. Thus, the input impedance Z_{in} can be obtained. The desired fields under an excitation of any magnitude voltage V_{in} can be obtained by multiplying the factor V_{in}/Z_{in} to the results obtained when I is set to one Ampere.

EMAP5 models load impedances Z_L as dielectric posts on tetrahedron edges. These posts have a finite conductivity given by,

$$\boldsymbol{s} = \frac{l}{Z_L S} \tag{34}$$

where l is its length, and S is the cross sectional area. If the load is treated as a lumped element, its contribution to the finite element matrix is as follows [11] (pp. 324-325),

$$[A^e] = \frac{l^2}{Z_L} \iint \{W\}\{W\}^T \boldsymbol{d}(x - x_L)(y - y_L)\, dx\, dy \quad (35)$$

where (x_L, y_L) is the position of the impedance load.

IV. MATRIX EQUATION SOLVER

EMAP5 uses the complex bi-conjugate gradient method (CBCG) to solve the final complex matrix equation, Equation (23). The major advantage of CBCG lies in its iterative nature and its ability to use the row-indexed method to store sparse matrices efficiently. The CBCG method was first introduced by Jacobs [16]. A brief outline of the algorithm is provided in the following section.

A. Complex Bi-Conjugate Gradient Method

Consider a complex matrix equation,

$$[M][x]=[b] \quad (36)$$

where [M] is an N×N complex matrix, and [b] and [x] are order-N complex column vectors. Both [M] and [b] are known while [x] is unknown. Four column vectors are defined as,

1. the residue, r,
2. the bi-residue, $\overline{r}$,
3. the direction vector, p,
4. the bi-direction vector, $\overline{p}$.

These vectors are initialized as,

$$r_0 = p_0 = b \quad (37)$$

$$\overline{r_0} = \overline{p_0} = b^* \quad (38)$$

where * denotes the complex conjugate. The Hermitian conjugate of M is,

$$M^H \equiv (M*)^T \quad (39)$$

where T denotes transpose. The inner product of two complex column vectors is defined as,

$$\langle p_1, p_2 \rangle \equiv (p_1*)^T p_2 \quad . \quad (40)$$

The following steps are repeated N times at most. For k=0, … , N-1, calculate the step-length parameter,

$$\boldsymbol{a}_k = \frac{\langle \overline{r_k}, r_k \rangle}{\langle \overline{p_k}, Mp_k \rangle} \quad . \quad (41)$$

The new solution estimate then becomes,

$$x_{k+1} = x_k + \boldsymbol{a}_k p_k \quad . \quad (42)$$

The new residue and bi-residue are calculated as,

$$r_{k+1} = r_k - \boldsymbol{a}_k Mp_k \quad (43)$$

$$\overline{r_{k+1}} = \overline{r_k} - \boldsymbol{a}_k^* M^H \overline{p_k} \quad . \quad (44)$$

The bi-conjugate coefficient is calculated using the following formula,

$$\boldsymbol{b}_k = -\frac{\langle M^H \overline{p_k}, r_{k+1} \rangle}{\langle \overline{p_k}, Mp_k \rangle} \quad . \quad (45)$$

The new direction and bi-direction vectors are given by,

$$p_{k+1} = r_{k+1} + \boldsymbol{b}_k p_k \quad (46)$$

$$\overline{p_{k+1}} = \overline{r_{k+1}} + \boldsymbol{b}_k^* \overline{p_k} \quad . \quad (47)$$

This iteration is continued until a termination condition is satisfied,

$$\frac{\|r_k\|_2}{\|b\|_2} \le TOL \quad (48)$$

where TOL is a number defining the tolerance. The best value of TOL depends on the problem for EMAP5. Typically, 1×10^{-3} is sufficient. The value of TOL is defined as a macro in the EMAP5 source code so it can be easily adjusted by the user.

B. Implementation

It is not necessary to explicitly add the two matrices on the left-hand side of Equation (23) in CBCG. The FEM matrix [A] is a sparse and symmetric matrix. The row-indexed scheme [17] is used to store it. The MoM coupled matrix is an asymmetric compact matrix. A full 2D array is used to store it. These two matrices are stored separately in order to make it is easier to obtain the Hermitian of the left-hand matrix. Since [A] is symmetric,

$$A^H = (A^T)^* = A^* \quad (49)$$

Thus, it is not necessary to search the non-zero elements column by column in [A] when Hermitian operations are present. Instead, the search is done row by row. The row-indexed scheme is very efficient in this case. While the coupled MoM matrix is not symmetric, exchanging its row index and column index will result in its transpose.
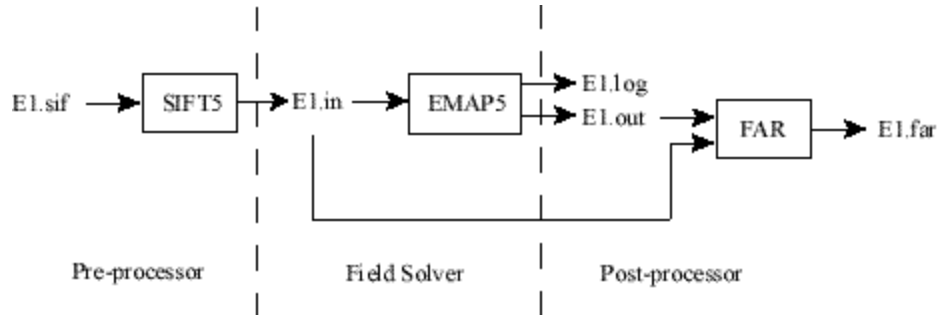
Figure 2. Components of the EMAP5 package.

C. Accuracy and Convergence Problem

Although the CBCG solver conserves memory, it is an iterative method and it may have difficulty converging in some situations. Convergence problems may result from round-off errors. Usually the round-off error for single-precision data is 1.19×10^{-7} [17]. If the total number of unknown edges is 1,000, the average error due to round-off errors is

$$\sqrt{1,000} \times 1.19 \times 10^{-7} \approx 3.8 \times 10^{-6} .$$

In the worst case, the error is $1,000 \times 1.19 \times 10^{-7} = 1.19 \times 10^{-4}$. Because the total round-off error could be very large, it is impractical to set the TOL in Equation (48) to be on the order of 10^{-4} if no special technique, such as pre-conditioning, is used to reduce the total round-off error. The round-off error of double-precision data is 2.22×10^{-16} [17]. If double precision is used for the matrix calculations, round-off errors will not reduce the effectiveness of CBCG considerably. In EMAP5, all data are stored in double precision; however, double precision numbers require twice as much as memory to store as single precision.

Another potential difficulty with the CBCG solver arises when the algorithm becomes unstable. This can happen when the denominator of the expressions for α_k and β_k is close to zero. EMAP5 monitors the value of the denominator. If it becomes too small, EMAP5 will restart the algorithm using the current solution as the initial estimate as suggested by Jacobs [16].

V. COMPONENTS OF EMAP5

EMAP5 is written in ANSI C. Thus, it can be compiled without modification on many computer platforms. As shown in Figure 2, the EMAP5 software package includes three major components: SIFT5, EMAP5 and FAR. EMAP5 was developed for research and educational use. It does not have a sophisticated mesh generator or graphical visualization tools. SIFT5 can be used to describe simple input geometries with a rectangular grid. It is also possible to use commercial mesh generators to analyze more complex geometries of arbitrary shape. EMAP5 is the FEM/MoM field solver. FAR calculates far-field electric fields from the equivalent surface currents calculated by EMAP5.

Standard Input File Translator version 5 (SIFT5) is designed to generate input files for the field solver EMAP5. SIFT5 reads a text file in the SIFT format [18-20] and generates an input file for EMAP5. Users can describe the structure of interest by using eleven keywords. The physical geometry of the structure, source type and location, and the geometry of areas in which fields are to be printed by the solver, must be specified.

EMAP5 is the hybrid FEM/MoM field solver. It reads an input file generated by SIFT5. A .log file is generated to log running status and error messages. The log file was initially designed to debug the code, but users can also benefit from log messages. EMAP5 will print out fields within areas specified by the .sif file, to one or more output files. All equivalent surface currents **J** and **M** must be printed to a file if the user needs to calculate far fields.

FAR is a program used to calculate the far field radiation pattern. FAR needs two input files. One is the file generated by SIFT5 and the other contains the equivalent surface currents **J** and **M**. The FAR program will prompt users to input the observing distance R in wavelengths, the observing θ interval in degrees, and the observing ϕ interval in degrees.

VI. STRUCTURE OF EMAP5

Figure 3 shows a flowchart for the field solver EMAP5. Descriptions of the functions used by EMAP5 are provided below,

- ReadInputFile()

   reads an input file generated by SIFT5, and checks whether the input file is consistent (i.e. the input makes sense). If not, it aborts the program and reports problems with the input to the user.

- ComputeBMatrix()

  places a 3×3 sub-matrix (corresponding to one observing triangular patch and one source triangular patch) into the global B matrix based on the local-to-global mapping.

- ComputeCMatrix()

  places a 3×3 sub-matrix into the global C matrix based on the local-to-global mapping.

- ComputeDMatrix()

  places a 3×3 sub-matrix into the global D matrix based on the local-to-global mapping.

- ComputeCorrectionTerm()

  uses B, C, and D matrices to compute the MoM coupling matrix. It also creates the necessary matrices required to compute the equivalent surface currents.

- FEMMatrixCompute()

  computes a 6×6 matrix for each tetrahedron first, then assembles the global matrix based on the local-to-global mapping. The matrix is stored using the row-indexed method.

- CreateRHSVector()

  creates the RHS (right-hand side) vector of the final matrix equation.

- ConjugateSolver()

  uses the Complex Bi-Conjugate Gradient Method to solve the final matrix equation. For MoM-only analyses, this function can be replaced with an LU decomposition solver.

- SurfaceFieldCompute()

  computes the equivalent surface currents on the boundary.

- PrintOutput()

  outputs the values of fields in regions specified by the input file to a file specified by the input file. All equivalent surface electric and magnetic currents must be written to a file if users are interested in the far field pattern.

VII. NUMERICAL RESULTS

This section describes four example geometries that can be solved using the EMAP5 software package. Each geometry is described in sufficient detail to allow others to duplicate the analysis. Results obtained from EMAP5 are compared to results obtained using other well-established codes, measurements, or analytical results.
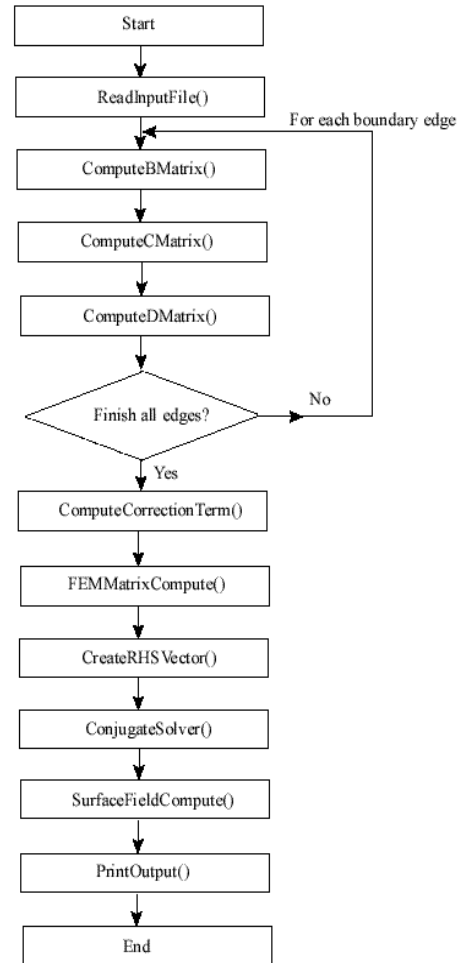

Figure 3. EMAP5 flowchart.

The first example analyzes the electromagnetic scattering from a square plate over a dielectric slab. As shown in Figure 4, the configuration consists of a square plate of dimension $0.75\lambda \times 0.75\lambda$, and a dielectric slab of $\varepsilon_r = 2.0$, and dimensions of $0.4\lambda \times 0.4\lambda \times 0.2\lambda$. The plate is symmetrically placed above the slab. The distance between the plate and the dielectric slab is 0.15λ. The system is illuminated by an x-polarized, +z traveling plane wave. In EMAP5's hybrid solution, the dielectric is divided into 320 tetrahedra. The surface of the dielectric and the metal plate are divided into 392 triangle patches. Figure 5 shows the normalized far field pattern calculated by EMAP5. For comparison, the results obtained by Arvas *et al.* [21] have been plotted on the same scale. The authors in [21] used a method of moments technique, which is based on a combined field integral equation formulation. As is evident from the figure, the two solutions compare very well.
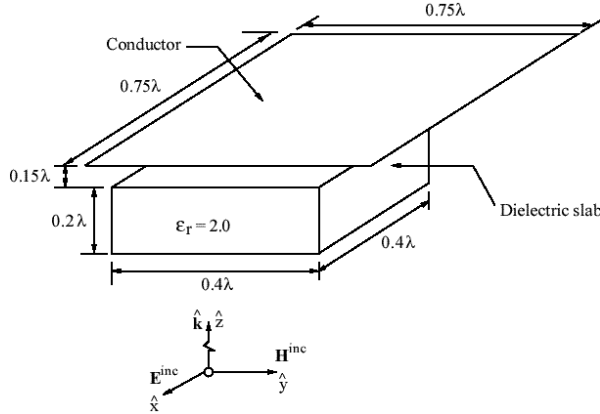
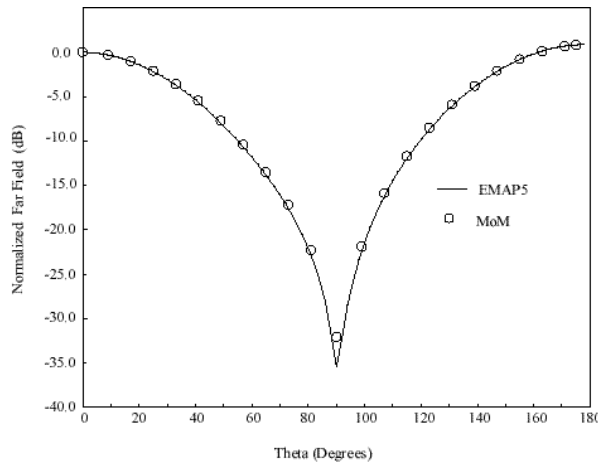Figure 4. A conducting plate over a dielectric slab.

Figure 5. The normalized far field pattern for the configuration in Figure 4.

The second example demonstrates the application of the EMAP5 code in mo deling microstrip geometries. The geometry of the structure is shown in Figure 6. The board is made of a dielectric with ε_r=4.0. The trace is excited by a source at one end, and is terminated by a resistor at the other end. Microstrip lines support quasi-TEM fields [22] (pp. 160-161) and can therefore be viewed as transmission lines. The input impedance Z_{in} of a transmission line is given by,

$$Z_{in} = Z_0 \frac{Z_L + j Z_0 \tan(\hat{a} l)}{Z_0 + j Z_L \tan(\boldsymbol{b} l)} \tag{50}$$

where Z_L is the load impedance, $\boldsymbol{b}$ is the propagation constant; l is the length of the transmission line. To determine the characteristic impedance Z_0 of the transmission line, one can find the input impedance when the load side is shorted or open, respectively. When the load side is shorted, the input impedance is given by,

$$\left(Z_{in}\right)_{short} = j Z_0 \tan(\boldsymbol{b} l) . \tag{51}$$

When the load side is open, the input impedance is given by,

$$\left(Z_{in}\right)_{open} = - j \frac{Z_0}{\tan(\boldsymbol{b} l)} . \tag{52}$$

Thus, the characteristic impedance is given by,

$$Z_0 = \sqrt{(Z_{in})_{short}(Z_{in})_{open}} . \tag{53}$$

In EMAP5's hybrid solution, the dielectric volume is divided into 900 tetrahedra. The surface is divided into 828 triangles. Table 1 lists $\left(Z_{in}\right)_{open}$, $(Z_{in})_{short}$ and Z_0 obtained using EMAP5 at three different frequencies. The results in Table 1 are consistent and $Z_0 = 56.4$ Ohms at each frequency. Figure 7 shows the input impedance at the source end obtained by EMSIM [23] when the trace is terminated with a 56.4 Ω resistor. It is evident that the microstrip line is almost perfectly matched confirming EMAP5's calculation of the characteristic impedance.
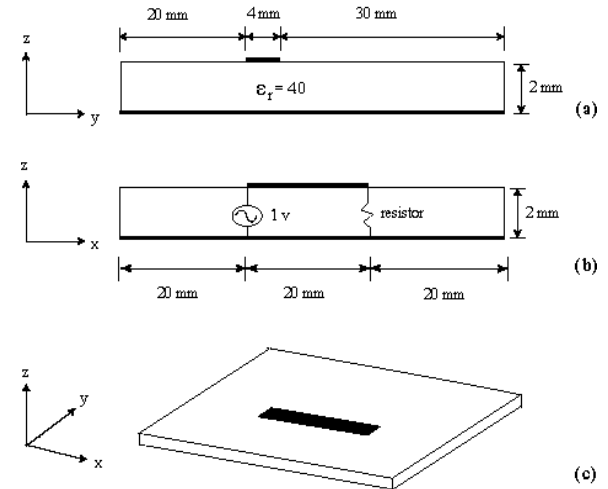

Figure 6. A microstrip geometry. (a) y-z plane view, (b) x-z plane view, and (c) 3D view.

Table 1. Impedances obtained using EMAP5.

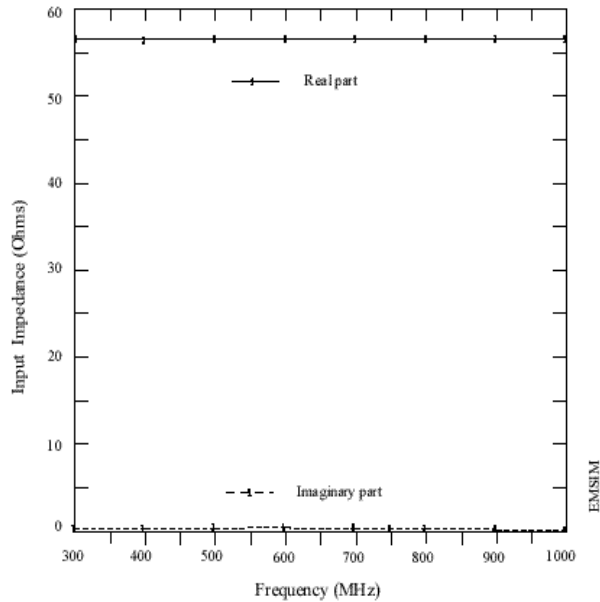| Source Frequency (MHz)	$\left(Z_{in}\right)_{open}$ (Ohms)	$(Z_{in})_{short}$ (Ohms)	Z_0 (Ohms)
300	-j187	+j17	56.4
500	-j106	+j30	56.4
700	-j69	+j46	56.3

Figure 7.   The input impedance obatined using EMSIM with a 56-Ohm load resistor.

The third example simulates the coupling between an active trace and an off-board trace on a printed circuit board. As shown in Figure 8, the active trace is excited by a 1-volt, 600 MHz source at one end, and is terminated by a 50-Ohm resistor at the other end. The off-board trace runs parallel to the active trace and extends well off the board. In EMAP5's hybrid solution, the dielectric volume is divided into 900 tetrahedra. The surface is divided into 876 triangles. For the first test case, there is no dielectric material between the traces and the ground. Therefore, the model contains only perfect electrical conductor (PEC) and can be analyzed using only the MoM portion of EMAP5. Figure 9 shows the current on the off-board trace obtained by EMAP5 compared with results obtained by EMSIM. For the second test case, the dielectric constant of the slab is set to 4.0. Figure 10 shows the results obtained by EMAP5 compared with results obtained using EMSIM. For both cases, good agreement is obtained between EMAP5 and EMSIM.

The fourth example models a printed circuit board power bus structure. As shown in Figure 11, the top and the bottom planes of the board are PEC. The dielectric between the top and bottom planes has a relative permittivity of 4.3(1-j0.02). Two test ports are identified at the locations shown in Figure 11. In EMAP5's hybrid solution, the dielectric volume is divided into 1,500 tetrahedra. The surface of the dielectric and the metal plates are divided into 1,340 triangle patches.   The model is verified using measurements of an actual printed circuit board with the dimensions shown in Figure 11. Two 85-mil semi-
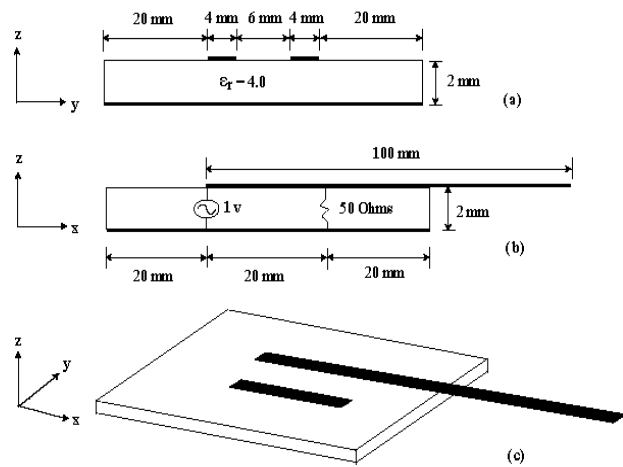

Figure 8. A grounded printed circuit board with active and passive traces. (a) y-z plane view, (b) x-z plane view, and (c) 3D view.
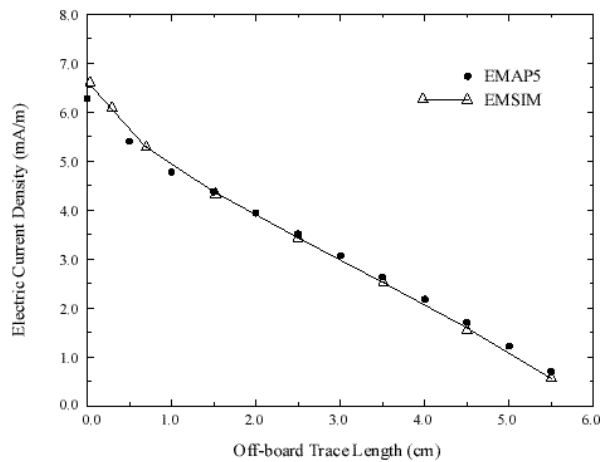

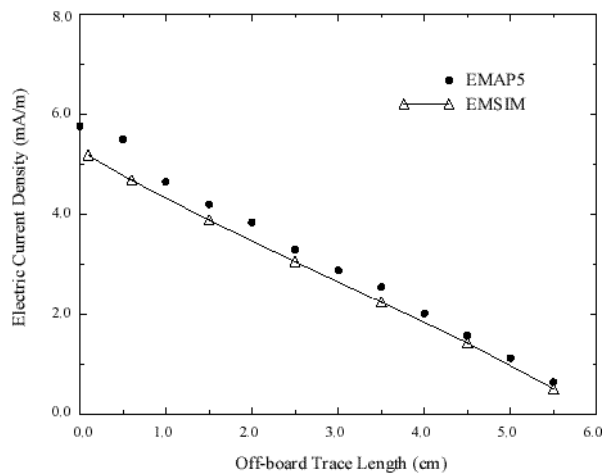Figure 9.   Current distribution on the off-board trace (ε_r =1.0).

Figure 10. Current distribution on the off-board trace (ε_r=4.0).

rigid coaxial probes are attached at the port locations. A network analyzer is used to measure the scattering parameters of the two-port system up to 2.0 GHz. The measured and modeled $|S_{11}|$ and $|S_{21}|$ results are plotted in Figure 12 and Figure 13, respectively.
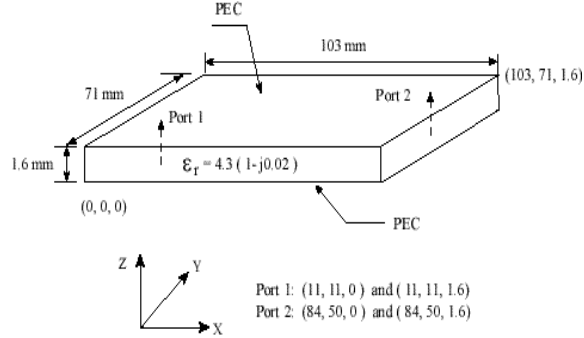

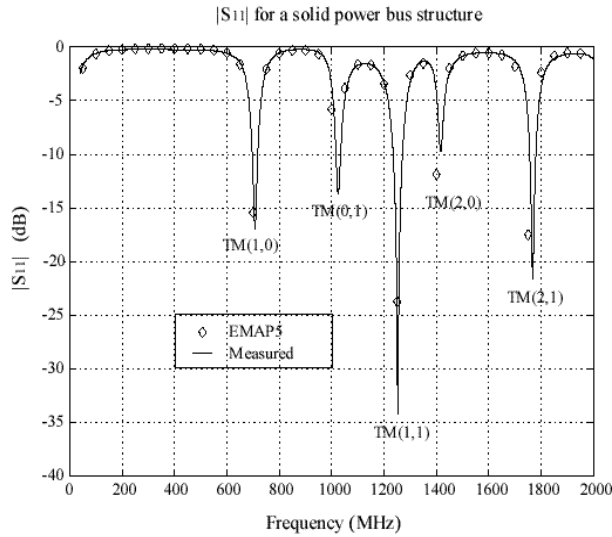Figure 11. A two-port power bus structure.

Figure 12.   The measured and calculated $|S_{11}|$ for the power bus structure.

The power bus structure can be analyzed as a cavity with two PEC and four perfect magnetic conductor (PMC) walls. The cutoff frequencies are given as follows (for lossless case and $\mu_r = 1.0$) [22],

$$f_c = \frac{c}{2\pi\sqrt{\varepsilon_r}}\sqrt{\left(\frac{m\pi}{a}\right)^2 + \left(\frac{n\pi}{b}\right)^2} \quad m,n = 0, 1, 2, \ldots \quad (54)$$

where a and b are the length and width of the cavity, respectively; m and n are the mode indices; c is the light speed in free space; ε_r is the relative permittivity of the material in the cavity. For this power bus structure, only TM_z modes are excited.

Table 2 lists the calculated cutoff frequencies of the first five TM_z modes. As shown in Figure 12, the $|S_{11}|$ response dips at these resonant frequencies. At resonance, more power is delivered to the board hence more power is transmitted to Port 2 as shown in Figure 13. The measurements, numerical results and theoretical analysis agree very well.
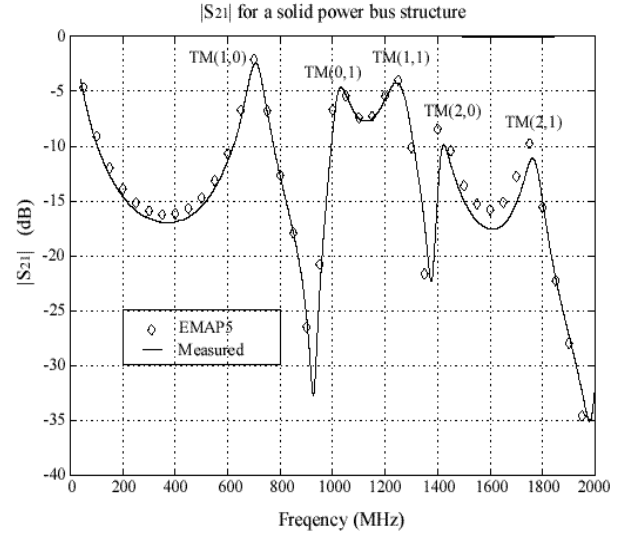

Figure 13. The measured and calculated $|S_{21}|$ for the power bus structure.

Table 2.   The TM_z mode cutoff frequencies of the power bus structure.

Mode	TM_z (1,0)	TM_z (0,1)	TM_z (1,1)	TM_z (2,0)	TM_z (2,1)
fc (GHz)	0.702	1.019	1.237	1.405	1.735

VIII. SUMMARY

The EMAP5 hybrid FEM/MoM code allows users to analyze geometries with large PEC surfaces and lossy dielectrics. Unlike codes that simply use the MoM surface as an absorbing boundary for the FEM region, EMAP5 can model PEC surfaces inside, outside and adjacent to the boundary between FEM and MoM regions. This permits a variety of interesting geometries to be modeled efficiently. The SIFT5 input translation code allows users to input simple 3D geometries to EMAP5 without a graphical user interface. Four sample geometries were analyzed that demonstrate the types of problems that can be analyzed

using SIFT5 and EMAP5. Good agreement was achieved between EMAP5 results and other well-established codes, analytical results, and measurements.

REFERENCES

[1]   R. F. Harrington, *Field Computation by Moment Methods*, pp. 1-9, New York: Macmillan, 1968.

[2]   D. G. Dudley, *Mathematical Foundations for Electromagnetic Theory*, pp. 33-36, New York: IEEE Press and Oxford University Press, 1994.

[3]   X. Yuan, D. R. Lynch, and J. W. Strohbehn, "Three-dimensional finite, boundary, and hybrid element solutions of the Maxwell's equations for lossy dielectric media," *IEEE Trans. on Microwave Theory and Tech.*, vol. 36, pp. 682-693, Apr. 1988.

[4]   J.-M. Jin and J. L. Volakis, "Electromagnetic scattering by and transmission through a three-dimensional slot in a thick conducting plane," *IEEE Trans. on Antennas and Propagat.*, vol. 39, pp. 543-550, Apr. 1991.

[5]   A. J. Sangster and H. Wang, "A combined FEM/MoM technique of coupling radiating apertures in rectangular waveguide," *IEEE Trans. on Magnetics*, vol. 31, pp. 1554-1557, May 1995.

[6]   M. W. Ali, T. H. Hubing, and J. L. Drewniak, "A hybrid FEM/MoM technique for electromagnetic scattering and radiation from dielectric objects with attached wires," *IEEE Trans. on Electromagnetic Compatibility*, vol. 39, pp. 304-314, Nov. 1997.

[7]   M. W. Ali, "Development of a hybrid 3D numerical modeling technique for analyzing printed circuit models with attached wires," Ph.D. dissertation, University of Missouri-Rolla, Dec. 1996.

[8]   A. F. Peterson, S. L. Ray, and R. Mittra, *Computational Methods for Electromagnetics*, pp. 461-463, New York: IEEE Press and Oxford University Press, 1997.

[9]   P. P. Silvester and R. L. Ferrari, *Finite Elements for Electrical Engineers*, 3rd edition, pp. 405-406 New York: Cambridge University Press, 1996.

[10] J. L. Volakis, A. Chatterjee, and L. C. Kempel, *Finite Element Method for Electromagnetics*, New York: IEEE Press and Oxford University Press, 1998.

[11] J.-M. Jin, *The Finite Element Method in Electromagnetics*, New York: John Wiley & Sons Inc, 1993.

[12] M. L. Barton and Z. J. Cendes, "New vector finite elements for three-dimensional magnetic field computation," *Journal of Applied Physics*, vol. 61, pp. 3919-3921, Apr. 1987.

[13] J. J. H. Wang, *Generalized Moment of Methods in Electromagnetics*, pp. 171-174, New York: John Wiley & Sons, 1990.

[14] S. M. Rao, D. R. Wilton, and A. W. Glisson, "Electromagnetic scattering by surfaces of arbitrary shape," *IEEE Trans. on Antennas and Propagat.*, vol. 30, pp. 409-418, May 1982.

[15] C. A. Balanis, *Advanced Engineering Electromagnetics*, 2nd edition, pp. 285-288, New York: John Wiley & Sons, 1989.

[16] D. A. H. Jacobs, "A generalization of the conjugate gradient method to solve complex systems," *IMA J. Numerical Anal.*, vol. 6, pp. 447-452, 1986.

[17] W. H. Press, S. A. Teukolsky, W. T. Vettering, and B. P. Flannery, *Numerical Recipes in C: The Art of Scientific Computing*, 2nd edition, New York: Cambridge University Press, 1992.

[18] T. H. Hubing, H-H. Lim, and J. L. Drewniak, "A geometry description language for 3D electromagnetic analysis codes," *Proceedings of the 10th Annual Review of Progress in Applied Computational Electromagnetics*, pp. 417-422, Mar. 1994.

[19] Y. Ji, "Enhancements to EMAP5", M.S. thesis, University of Missouri-Rolla, Dec. 1997.

[20] EMAP5 web page at http://www.emclab.umr.edu/emap5.

[21] E. Arvas, A. Rahhal-Arabi, and A. Sadigh, "Scattering from multiple conducting and dielectric bodies of arbitrary shape," *IEEE Antenna and Propagation Magazine*, vol. 33, No. 2, Apr. 1991.

[22] D. M. Pozar, *Microwave Engineering*, 2nd edition, New York: John Wiley & Sons Inc, 1998.

[23] EMSIM is a 3D numerical electromagnetic modeling code marketed by Pacific Numerix, Scottsdale, AZ, http://www.pnc.com.

Appendix A. Evaluation of B Matrix

The elements in B are given by,

$$B_{mn} = \int_{S_m} \mathbf{w}_m(\mathbf{r}) \bullet \mathbf{f}_n(\mathbf{r}) \, dS . \qquad \text{(A-1)}$$

When edge m and n do not lie on a common triangle, B_{mn} is zero. In addition, $B_{mn} = 0$ when $m=n$, because

$$\mathbf{w}_n(\mathbf{r}) = \hat{\mathbf{n}} \times \mathbf{f}_n(\mathbf{r}). \qquad \text{(A-2)}$$

If edge m and n lie on a common triangle T^q, B_{mn} is given by,

$$B_{mn} = \int_{S_m} \mathbf{w}_m(\mathbf{r}) \bullet \mathbf{f}_n(\mathbf{r}) \, dS = \int_{S_m} [\hat{\mathbf{n}} \times \mathbf{f}_m(\mathbf{r})] \bullet \mathbf{f}_n(\mathbf{r}) \, dS$$

$$= \int_{S_m} \hat{\mathbf{n}} \bullet [\mathbf{f}_m(\mathbf{r}) \times \mathbf{f}_n(\mathbf{r})] \, dS = \hat{\mathbf{n}} \bullet \int_{S_m} [\mathbf{f}_m(\mathbf{r}) \times \mathbf{f}_n(\mathbf{r})] \, dS$$

$$= \left(\frac{\pm l_m}{2A^q} \right) \left(\frac{\pm l_n}{2A^q} \right) \hat{\mathbf{n}} \bullet \int_{S_m} [(\mathbf{r} - \mathbf{r}_m) \times (\mathbf{r} - \mathbf{r}_n)] \, dS$$

$$= \left(\frac{\pm l_m}{2A^q} \right) \left(\frac{\pm l_n}{2A^q} \right) \hat{\mathbf{n}} \bullet \int_{S_m} [\mathbf{r}_m \times \mathbf{r}_n + (\mathbf{r}_n - \mathbf{r}_m) \times \mathbf{r}] \, dS . \quad \text{(A-3)}$$

The $\pm$ signs before l_m and l_n refer to the edge directions of edge m and edge n, respectively. The integral term in Equation (A-3) can be evaluated using the one-point Gaussian Quadrature technique,

$$B_{mn} = \frac{(\pm l_m)(\pm l_n)}{4A^q} \hat{\mathbf{n}} \bullet \left[\mathbf{r}_m \times \mathbf{r}_n + (\mathbf{r}_n - \mathbf{r}_m) \times \mathbf{r}^{cp} \right] \quad \text{(A-4)}$$

where $\mathbf{r}^{cp}$ is the centroid of triangle T^q.

Appendix B. Evaluation of Matrix D

The elements in matrix D are given by,

$$D_{mn} = \int_{S_m} \mathbf{f}_m(\mathbf{r}) \bullet \left[\oint_{S_n} \mathbf{f}_n(\mathbf{r}') \times \nabla' G_0(\mathbf{r},\mathbf{r}') dS' + \frac{1}{2} \mathbf{w}_n(\mathbf{r}) \right] dS$$

$$= -\frac{1}{2} B_{mn} + D'_{mn} \quad (\text{since } B_{mn} = -B_{nm}) \qquad \text{(B-1)}$$

where D'_{mn} is defined as follows,

$$D'_{mn} = \int_{S_m} \mathbf{f}_m(\mathbf{r}) \bullet \left[\oint_{S_n} \mathbf{f}_n(\mathbf{r}') \times \nabla' G_0(\mathbf{r},\mathbf{r}') dS' \right] dS$$

$$= \left(\frac{\pm l_m}{2A^m} \right) \left(\frac{\pm l_n}{2A^n} \right) \int_{S_m} (\mathbf{r} - \mathbf{r}_m) \qquad \text{(B-2)}$$

$$\bullet \left[\oint_{S_n} (\mathbf{r}' - \mathbf{r}'_n) \times \nabla' G_0(\mathbf{r},\mathbf{r}') dS' \right] dS$$

$$\nabla' G_0(\mathbf{r},\mathbf{r}') = \frac{1 + j k_0 R}{4 \boldsymbol{p} R^3} e^{-jk_0 R} \mathbf{R} \qquad \text{(B-3)}$$

where $\mathbf{R} = \mathbf{r} - \mathbf{r}'$, $R = |\mathbf{R}|$. The $\pm$ signs before l_m and l_n refer to the edge directions of edge m and edge n, respectively. Because the EFIE given by Equation (8) already excludes the singularity at $\mathbf{r} = \mathbf{r}'$, D'_{mn} can be evaluated directly using the seven-point Gaussian Quadrature technique.